

# CONSISTENT POSTERIOR DISTRIBUTIONS UNDER VESSEL-MIXING: A REGULARIZATION FOR CROSS-DOMAIN RETINAL ARTERY/VEIN CLASSIFICATION

Chenxin Li, Yunlong Zhang, Zhehan Liang, Wenao Ma, Yue Huang, Xinghao Ding

Xiamen University

## ABSTRACT

Retinal artery/vein (A/V) classification is a critical technique for diagnosing diabetes and cardiovascular diseases. Although deep learning based methods achieve impressive results in A/V classification, their performances usually degrade severely when being directly applied to another database, due to the domain shift, e.g., caused by the variations in imaging protocols. In this paper, we propose a novel vessel-mixing based consistency regularization framework, for cross-domain learning in retinal A/V classification. Specially, to alleviate the severe bias to source domain, based on the label smooth prior, the model is regularized to give consistent predictions for unlabeled target-domain inputs that are under perturbation. This consistency regularization implicitly introduces a mechanism where the model and the perturbation is opponent to each other, where the model is pushed to be robust enough to cope with the perturbation. Thus, we investigate a more difficult opponent to further inspire the robustness of model, in the scenario of retinal A/V, called vessel-mixing perturbation. Specially, it effectively disturbs the fundus images especially the vessel structures by mixing two images regionally. We conduct extensive experiments on cross-domain A/V classification using four public datasets, which are collected by diverse institutions and imaging devices. The results demonstrate that our method achieves the state-of-the-art cross-domain performance, which is also close to the upper bound obtained by fully supervised learning on target domain.

**Index Terms**— Cross-domain learning, retinal A/V classification, unsupervised domain adaptation

## 1. INTRODUCTION

The clinical features in retinal arteries and veins (A/V) serve as biomarkers in diagnosing many systemic and cardiovascular diseases [1]. However, labeling retinal A/V by a human observer is generally time-consuming and prone to human errors, since the vessel structures are usually complicated, which makes the automated retinal A/V classification highly desirable. Conventional machine learning based methods usually start from a pre-segmented vascular tree, and then extract hand-crafted features or incorporate the graphical con-

nection information to learn a classifier for vessel pixels [1, 2, 3]. Recently, several deep learning based works simultaneously segment and classify retinal A/V [4, 5, 6], employing the deep semantic-segmentation models that are trained on the well-annotated fundus images.

Despite of their success, they all neglect the potential domain shift existed between training and testing dataset. An example is using the model trained on the fundus images from one medical institution, to segment A/V on the images from another institution. The datasets are collected from different institutions and imaging devices, and appear in various field-of-view, resolution and light intensity [7] (cf. Fig.1). There exists a non-negligible domain shift across the datasets, so they should be considered as cross-domain data, which brings the degradation of evaluation performance. With the additional need for only unlabeled target data, recent unsupervised domain adaptation (UDA) seems more appealing in medical image segmentation [8, 9, 10, 11] These methods can be divided into two streams. One category extracts domain-invariant features by minimizing the inter-domain discrepancy [8, 9]. However, as discussed in [12, 11], different from classification task, the alignment of high-dimensional feature maps in segmentation task may also harm the contained structure information, and further cause negative transfer (c.f. Tab. 1). This could be worse for retinal A/V in fundus images where the complicated graphical structures of vessels contain more refined structure information (cf. Fig. 1).

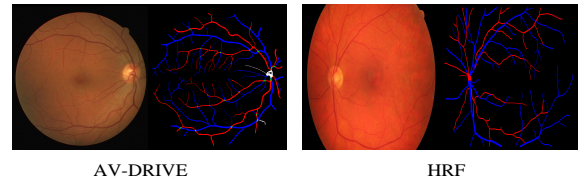


**Fig. 1.** Retinal fundus images and A/V annotations. In annotations, red, blue, green denote artery, vein and crossing pixel, respectively.

Another stream, which our method is based on, introduces the scheme of consistency regularization from semi-supervised learning into UDA [10, 11]. Based on the label smooth prior, i.e., the samples close to each other are ex-

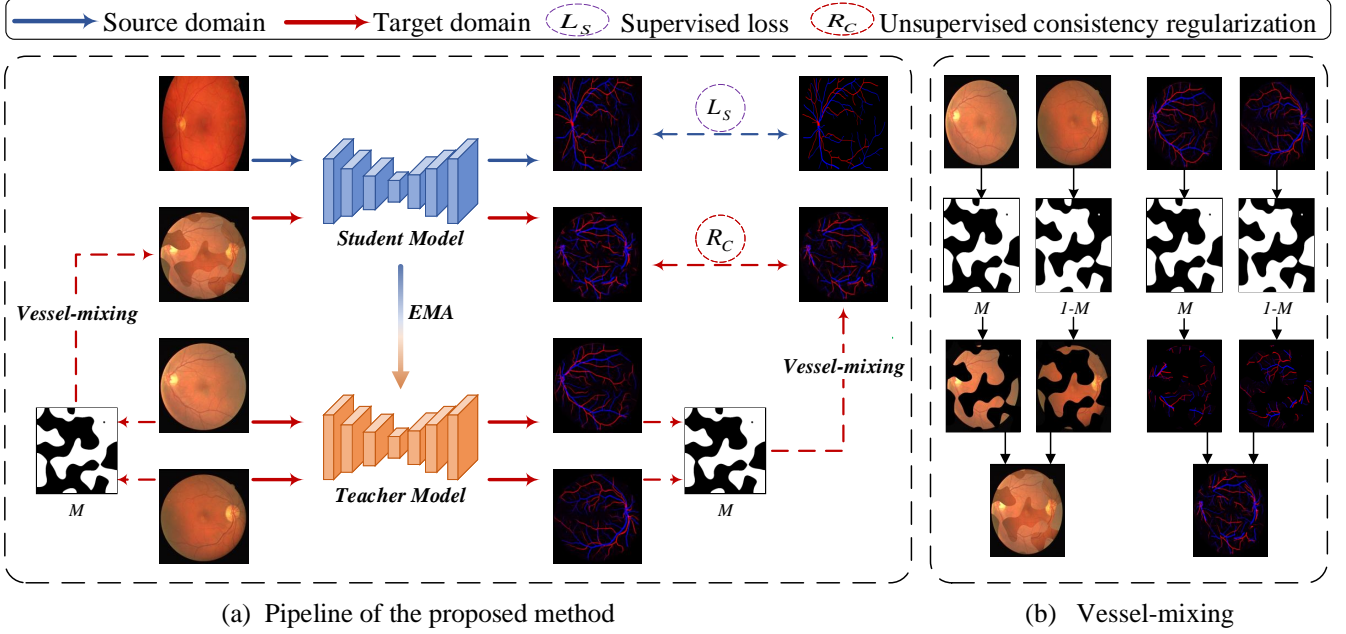


**Fig. 2.** The pipeline of the proposed vessel-mixing based consistency regularization. *EMA* in (a) means the exponential moving average of the student model’s weights are transferred to the teacher model’s weights [15]. *Vessel-mixing* in (a) is shown in (b) in detail.

pected to have the same label [13, 14], the regularization encourages the consistent pixel-level predictions for unlabeled target-domain inputs that are perturbed. It implicitly constructs an opponent mechanism for model and image perturbation, where the model is pushed to keep robustness enough against the perturbation. So we consider to utilize a more powerful perturbation, to inspire a more robust model.

In this paper, for the retinal A/V classification in cross-domain scenario, which still remains to be developed, we propose the novel vessel-mixing based consistency regularization. First of all, the framework regularizes the model to give consistent A/V prediction maps for the target-domain inputs that are perturbed, to underline the robustness of model. More importantly, we specifically develop a more powerful perturbation in the scenario of retinal A/V, to push the model to be more robust against it. That is vessel-mixing, which regionally mixes the vessel structures from two fundus images.

## 2. METHOD

The proposed framework is shown in Fig. 2. We assume that we are given a set of fundus images  $x_s$  along with their pixel-wise A/V annotations  $y_s$ , and a set of unannotated fundus images  $y_t$ . The former is regarded as source domain and the latter as target domain.

### 2.1. Basic consistency regularization framework

The unsupervised consistency regularization is carried out on target-domain data, which constrains the model to give consistent prediction maps for the inputs under some perturbations. For example, as shown in Fig. 3, the consistency regularization works for medical image segmentation [10, 11] usually employ spatial transformation (e.g., flipping, rotation, etc.) as the perturbation. Then a mean-squared error (MSE) loss to measure the consistency of model predictions under the disturbance, formulated as:

$$\mathcal{R}_C = \mathcal{L}_{mse}(f_{\theta}(g_{\phi}(x_t)), g_{\phi}(f_{\theta'}(x_t))) \quad (1)$$

The former term in the MSE loss represents the model predictions for the transformed inputs, and the latter denotes the transformed predictions for the origin inputs, where  $f$  denotes the mapping function of model with parameters  $\theta$  or  $\theta'$ .  $g$  denotes the spatial transformation with parameters  $\phi$ . Note that the model parameter  $\theta$  and  $\theta'$  is different, respectively for the student model and teacher model. It is called *Mean Teacher* framework, which is proposed in [15, 16], and reported to improve the effect of consistency regularization with only a single model. Concretely, the student model is trained by routine gradient descent, and the exponential moving average (EMA) of the student’s weights  $\theta$  is then transferred to the teacher model’s weights  $\theta'$ :  $\theta'_t = \alpha\theta'_{t-1} + (1 - \alpha)\theta_t$ , where  $t$  means the state of training step  $t$ ,  $\alpha$  is the EMA decay that controls the transfer rate, usually set 0.99 in most related

works [10, 11, 15, 13].

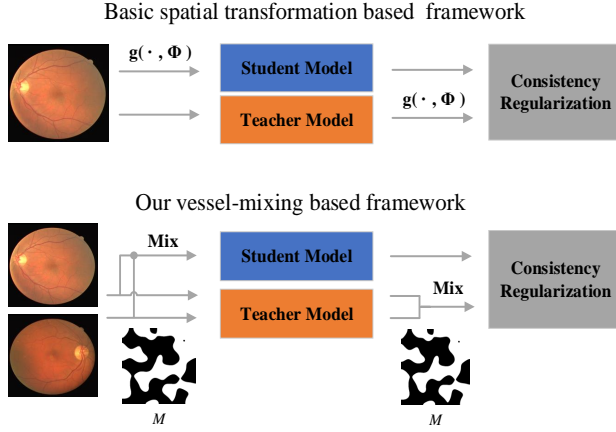


**Fig. 3.** The comparison between the flowcharts of perturbation-based consistency regularization methods.  $g(\cdot, \phi)$ : the spatial transformation with parameter  $\phi$ .  $Mix$ : the proposed vessel-mixing perturbation.

## 2.2. Vessel-mixing based consistency regularization

### 2.2.1. Motivation

Since the opponent mechanism built by consistency regularization where the perturbation is opponent to push the model to be better, a strong enough perturbation is essential [15, 13, 14]. Our insight is if a perturbation can appropriately affect the complicated graphical structures of retinal A/V, it may disturb the predictions more and perform a stronger perturbation. However, the crude perturbation of spatial transformation, such as flip, may lack the discussed ability. So we design a novel vessel-mixing perturbation to meet the challenge, which can significantly affects the vessel structures by mixing two fundus images. The recently proposed *Mixup* is a augmentation technique that mixes two images globally for classification task. But we think it is inappropriate to directly applying this in semantic segmentation where pixel-level information is important. So we develop the vessel-mixing perturbation, which mixes two fundus images in region-level.

### 2.2.2. Mechanism

First of all, we obtain a reference mask to guide mixing. Since the requirement of randomness, we starts from sampling a Gaussian random matrix with the same size as the images to be mixed, and then apply Gaussian filter to introduce regional correction. At last, the value in each location is binarized with a threshold, which is the mean value of matrix in our case. Given the mask  $M$ , the input images  $x_{t1}$  and  $x_{t2}$ , the mixture is obtained by:

$$Mix(x_{t1}, x_{t2}, M) = M \odot x_{t1} + (\mathbb{1} - M) \odot x_{t2} \quad (2)$$

where  $\odot$  represents Hadamard product. Similar to Eq.1, which regularizes the consistency between the predictions of transformed input and the transformed predictions of origin input, here we also adopt the same form of consistency regularization, regarding the mix operation as a special transformation, as:

$$Mix(f_{\theta'}(x_{t1}), f_{\theta'}(x_{t2}), M) = M \odot f_{\theta'}(x_{t1}) + (\mathbb{1} - M) \odot f_{\theta'}(x_{t2}) \quad (3)$$

$$\mathcal{R}_C = \mathcal{L}_{mse}(f_{\theta}(Mix(x_{t1}, x_{t2}, M)), Mix(f_{\theta'}(x_{t1}), f_{\theta'}(x_{t2}), M)) \quad (4)$$

## 2.3. Overall loss function

In our whole framework, the training dataflow is split to source domain and target domain. For labeled source data, we apply the sum of cross-entropy (BCE) losses respectively for arteries and veins, since there always exists the crossings pixels of arteries and veins in retinal fundus images, which are labeled as both classes. Also, to alleviate the class imbalance problem between the foreground and background, we set a positive weight  $w_{pos}$  as 10. The supervised loss is formulated as:

$$\mathcal{L}_S = \mathcal{L}_{bce}^a(f_{\theta}(x_s), y_s, w_{pos}) + \mathcal{L}_{bce}^v(f_{\theta}(x_s), y_s, w_{pos}) \quad (5)$$

where  $a$  and  $v$  denotes A/V. For unlabeled target data, the consistency regularization loss introduced above is applied. Finally, the student model is trained by the weight sum of supervised loss and unsupervised regularization loss, as:

$$\mathcal{L} = \mathcal{L}_S + \lambda \mathcal{R}_C \quad (6)$$

where  $\lambda$  is the trade-off parameter that controls the training bias to the regularization term. We hope it can be self-adaptive according to the progress of training. When the model predicts the target-domain data with higher confidence, we think the consistency regularization can be more reliable. So we update  $\lambda$  by averaged threshold confidence: in the prediction maps of target-domain data (i.e., the output of teacher model), calculate the proportion of pixel-level predictions over threshold 0.97.

## 3. EXPERIMENTS

### 3.1. Dataset

We evaluate the proposed method by using four public color retinal fundus images datasets. These include AV-DRIVE [17], High Resolution Fundus (HRF) [18], LES-AV [19] and INSPIRE-AVR [20]. These datasets are collected by different institutions and devices, causing the domain shift among the datasets. The AV-DRIVE dataset has 20/20 (training/testing) images with resolution of 584×565, and publicly available pixel-wise labeling of A/V classification. The HRF database

**Table 1.** The results of A/V classification on four cross-database tasks.  $\rightarrow$  denotes *Source* adapted to *Target* under regular UDA protocols. *Source-only* denotes the evaluation results of models only trained on source data. *Target-only* denotes the results in supervised setting. UA-AV [7] and MT-AV [5] are the existing works for cross-domain retinal A/V classification without domain-adaptation techniques, which shows the cross-domain performance degradation and the necessity of applying UDA here. *Target-only* in D $\rightarrow$ I is lacking because INSPIRE has only centerline annotations that can't be used for supervised learning. Please note that here we evaluate A/V-classification performance on the ground truth vessels pixels, which is a more strict criteria, following [5, 7, 6]. In addition, AVNet is the fully supervised performance of a very recent state-of-the-art deep method, which is under the same criteria as ours and as the validity confirm for our *Target-only*.

Method	H $\rightarrow$ D	L $\rightarrow$ D
	F1/Acc/Sen/Sp	F1/Acc/Sen/Sp
Source-only	79.5/83.0/76.2/88.6	75.2/75.2/82.4/69.2
AdvNet [8]	81.0/83.2/81.0/85.3	74.9/76.5/77.8/75.4
PnP-AdaNet [9]	84.3/85.8/85.0/86.6	77.7/79.7/78.4/80.9
ST-CR [10]	86.2/87.8/86.6/88.9	83.0/84.1/85.7/83.1
<b>VM-CR(Ours)</b>	<b>87.6/89.1/86.8/91.1</b>	<b>84.3/85.5/85.6/85.7</b>
Target-only	89.1/90.2/89.1/91.2	89.1/90.2/89.1/91.2
AVNet [6]	— /90.6/88.3/90.6	— / — / — / —

Method	D $\rightarrow$ L	D $\rightarrow$ I
	F1/Acc/Sen/Sp	F1/Acc/Sen/Sp
Source-only	79.5/82.0/77.5/85.6	80.5/80.0/82.2/78.6
UA-AV [7]	86 / 86 / 88 / 85	80 / 80 / 82 / 87
MT-AV [5]	— / — / — / —	— /90.3/91.4/89.7
AdvNet [8]	80.6/81.6/83.8/80.0	84.8/84.1/83.4/85.5
PnP-AdaNet [9]	83.2/85.3/80.4/89.6	86.9/86.0/84.6/88.0
ST-CR [10]	86.1/86.8/89.7/84.6	91.3/90.6/88.4/93.0
<b>VM-CR(Ours)</b>	<b>87.5/88.5/88.2/88.9</b>	<b>92.5/92.2/94.5/90.5</b>
Target-only	89.1/89.5/90.3/88.9	— / — / — / —
AVNet [6]	— /90.0/90.3/91.2	— / — / — / —

contains 45 images of dimensions 1200 $\times$ 800, with a regular split of 23/22 and pixel-level annotations. The LES-AV dataset contains 22 optic-disc centered images with a resolution of 1620 $\times$ 1444 pixels, with a split of 11/11. INSPIRE-AVR contains 40 images of size 2048 $\times$ 2392, with A/V labels available only for centerline rather than pixel-wise annotations, so it can only be used for evaluation. For simplicity, we respectively denote: AV-DRIVE (D), HRF (H), LES-AV (L), INSPIRE-AVR (I).

### 3.2. Implementation details

We employ the U-Net architecture that are slightly adapted for retinal A/V classification in [5] as the backbone, for both teacher model and student model. In the training stage, we

sample a new mask  $M$  every iteration. we adopt Adam optimizer with a constant learning rate of 0.001 to optimize the student model. Each mini-batch contains 2 source-domain samples and 2 target-domain samples. We resize the input images to a common resolution of 512 $\times$ 512, and normalize them to [0, 1]. The standard data augmentation is applied to avoid overfitting, including random flipping, rotating and scaling. The total training iterations is 10000. In the testing stage, we use only the teacher model without *Mix* module. We implement the experiments in Pytorch, a NVIDIA Titan Xp GPU.

### 3.3. Experimental results

We adopt four metrics to quantitatively evaluate A/V classification performance: the average accuracy (Acc), sensitivity (Sen), specificity (Sp) and F1-score (F1), with arteries regarded as the positives and veins as the negatives. Following [5], we evaluate A/V classification performance on the ground truth vessels pixels rather than the segmented vessels, which is more strict since some capillary vessels may be not well segmented.

We report experimental results of the proposed method on four cross-database experiments Tab. 1. We compare our proposed method with several UDA-segmentation methods, AdvNet [8], PnP-AdaNet [9] and ST-CR [10]. We use the publicized codes of the compared models provided by their authors and adjust them to the same backbone with us for fair comparison. Meanwhile, the first two are the recently proposed domain-align based methods. ST-CR and VM-CR stand for the spatial transformation based consistency regularization and the proposed vessel-mixing consistency regularization, respectively. The main difference is the different perturbation for consistency regularization, and ST-CR can also be regarded as the baseline of our VM-CR. Moreover, to show degree of cross-domain performance degradation and the necessity of applying UDA here, we also report the results of the existing few works that conduct cross-domain retinal A/V classification without domain-adaptation techniques: UA-AV [7] and MT-AV [5]. In detail, UA-AV [7] is trained on AV-DRIVE, and MT-AV [5] is trained on AV-DRIVE and HRF.

First, we observe in no matter which cross-database task, *Source-only* suffers heavy performance degradation compared to *Target-only*. For example, in L $\rightarrow$ D, the degradation performance gap is 13.9% at F1, 15.0% at Acc, 22.0% at Sp, showing the need for paying great attention to the domain shift here. The three domain alignment methods achieve small improvements in several tasks, but we find AdaNet achieves even worse F1 score than Source-only in L $\rightarrow$ D, confirms our concern about *negative transfer* that may be caused by enforcing the high-dimensional feature maps of semantic segmentation task. The consistency regularization methods achieve significant improvements, showing the importance of improving the robustness of model in cross-domain retinal

A/V classification tasks. Moreover, the proposed VM-CR not only significantly outperforms Source-only, but also achieves very close performance to the Target-only. For example, we improve the F1 score to 87.6% and Acc to 89.1%, in H→D task, where Target-only achieves 89.1% for F1 and 90.2% for Acc. Also, our proposed VM-CR achieves the state-of-the-art performance in all the four cross-database tasks. Fig. 4 shows the visual results in H→D task. The proposed method segments and classifies most of the vessels accurately, which significantly improves the classification of A/V over Source-only, especially for the marked challenging regions.

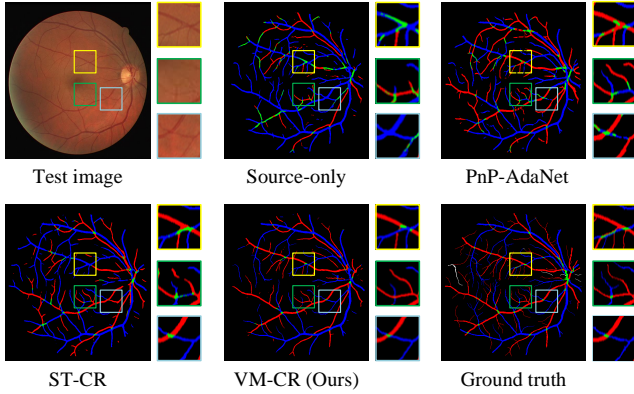


**Fig. 4.** Visual results of the UDA methods on cross-dataset A/V classification for H→D task. Note that we enlarge the views of several representative challenging regions.

### 3.4. Effectiveness analysis

The proposed method is from the insight that the consistency regularization framework implicitly introduces the opponent mechanism between the model and the perturbation, which pushes the model to be robust enough to give consistent predictions against the perturbation. Thus, we compare the proposed vessel-mixing based consistency regularization (VM-CR) and the spatial transformation based consistency regularization (ST-CR) baseline. We first observe the consistency loss map for a perturbation, which is the pixel-level distance between the predictions for perturbed input (i.e., the output of student model) and the perturbed predictions for origin input (i.e., the output of teacher model), in the early training stage. Specially, the numeric values in the corresponding loss map show the degree of perturbation on the model predictions. As shown in Fig. 5, the pixel values of consistency loss map for spatial transformation are almost all small, especially for flip, which means the spatial transformation performs a relatively weak perturbation for model. Instead, the proposed vessel-mixing perturbs the predictions more significantly, and also has more variety brought by randomly mixing in region-level. Thus, the more powerful vessel-mixing perturbation is a more difficult opponent for the model, and thus pushes the

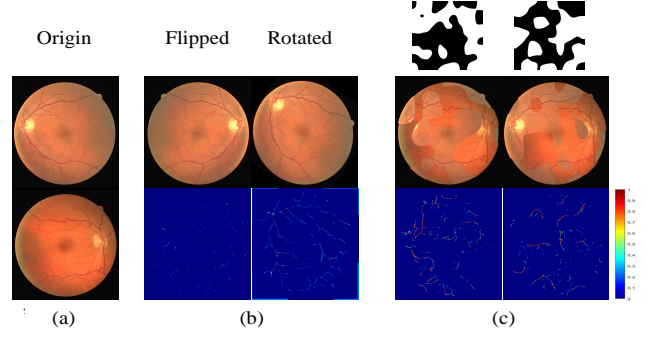


**Fig. 5.** The consistency loss maps, defined as the pixel-level squared-error loss between the predictions for perturbed input and the perturbed predictions for origin input. (a): the input images A and B. (b)(c): the perturbed input images and the loss maps. In detail, (b) is perturbed by the spatial transformation, e.g., flip or rotation, (c) is perturbed by the proposed vessel-mixing, with the randomly sampled masks  $M$ .

model to be more robust and better. As shown in Tab. 1 and Fig. 4, our proposed VM-CR outperforms ST-CR, with a significantly gap.

## 4. CONCLUSION

In this paper, we propose a novel vessel-mixing based consistency regularization, to for cross-domain retinal A/V classification. The consistency regularization framework constrains the model to give consistent A/V prediction maps for the unlabeled target inputs that are perturbed, to underline the robustness of model. Furthermore, we specifically develop vessel-mixing, which regionally mixes two images and contributes to a powerful perturbation, and thus further inspires a more robust model. The extensive experiments of cross-database A/V classification show that the proposed approach achieves the state-of-the-art performance.

## 5. REFERENCES

- [1] Rolando Estrada, Michael J Allingham, Priyatham S Mettu, Scott W Cousins, Carlo Tomasi, and Sina Farsiu, “Retinal artery-vein classification via topology estimation,” *IEEE transactions on medical imaging*, vol. 34, no. 12, pp. 2518–2534, 2015.
- [2] Xiayu Xu, Wenxiang Ding, Michael D Abràmoff, and Ruofan Cao, “An improved arteriovenous classification method for the early diagnostics of various diseases in retinal image,” *Computer methods and programs in biomedicine*, vol. 141, pp. 3–9, 2017.
- [3] Yitian Zhao, Jianyang Xie, Huaizhong Zhang, Yalin Zheng, Yifan Zhao, Hong Qi, Yangchun Zhao, Pan Su,



- Jiang Liu, and Yonghuai Liu, "Retinal vascular network topology reconstruction and artery/vein classification via dominant set clustering," *IEEE Transactions on Medical Imaging*, vol. 39, no. 2, pp. 341–356, 2019.
- [4] Maria Ines Meyer, Adrian Galdran, Pedro Costa, Ana Maria Mendonça, and Aurélio Campilho, "Deep convolutional artery/vein classification of retinal vessels," in *International Conference Image Analysis and Recognition*. Springer, 2018, pp. 622–630.
- [5] Wenao Ma, Shuang Yu, Kai Ma, Jiexiang Wang, Xinghao Ding, and Yefeng Zheng, "Multi-task neural networks with spatial activation for retinal vessel segmentation and artery/vein classification," in *International Conference on Medical Image Computing and Computer-Assisted Intervention*. Springer, 2019, pp. 769–778.
- [6] Hong Kang, Yingqi Gao, Song Guo, Xia Xu, Tao Li, and Kai Wang, "Avnet: A retinal artery/vein classification network with category-attention weighted fusion," *Computer Methods and Programs in Biomedicine*, vol. 195, pp. 105629, 2020.
- [7] Adrian Galdran, M Meyer, P Costa, A Campilho, et al., "Uncertainty-aware artery/vein classification on retinal images," in *2019 IEEE 16th International Symposium on Biomedical Imaging (ISBI 2019)*. IEEE, 2019, pp. 556–560.
- [8] Konstantinos Kamnitsas, Christian Baumgartner, Christian Ledig, Virginia Newcombe, Joanna Simpson, Andrew Kane, David Menon, Aditya Nori, Antonio Criminisi, Daniel Rueckert, et al., "Unsupervised domain adaptation in brain lesion segmentation with adversarial networks," in *International conference on information processing in medical imaging*. Springer, 2017, pp. 597–609.
- [9] Qi Dou, Cheng Ouyang, Cheng Chen, Hao Chen, Ben Glocker, Xiahai Zhuang, and Pheng-Ann Heng, "Pnp-adanet: Plug-and-play adversarial domain adaptation network with a benchmark at cross-modality cardiac segmentation," *arXiv preprint arXiv:1812.07907*, 2018.
- [10] Christian S Perone, Pedro Ballester, Rodrigo C Barros, and Julien Cohen-Adad, "Unsupervised domain adaptation for medical imaging segmentation with self-ensembling," *NeuroImage*, vol. 194, pp. 1–11, 2019.
- [11] Peng Liu, Bin Kong, Zhongyu Li, Shaoting Zhang, and Ruogu Fang, "Cfea: Collaborative feature ensembling adaptation for domain adaptation in unsupervised optic disc and cup segmentation," in *International Conference on Medical Image Computing and Computer-Assisted Intervention*. Springer, 2019, pp. 521–529.
- [12] Yang Zhang, Philip David, and Boqing Gong, "Curriculum domain adaptation for semantic segmentation of urban scenes," in *Proceedings of the IEEE International Conference on Computer Vision*, 2017, pp. 2020–2030.
- [13] Samuli Laine and Timo Aila, "Temporal ensembling for semi-supervised learning," *arXiv preprint arXiv:1610.02242*, 2016.
- [14] Geoff French, Timo Aila, Samuli Laine, Michal Mackiewicz, and Graham Finlayson, "Semi-supervised semantic segmentation needs strong, high-dimensional perturbations," *arXiv e-prints*, p. arXiv:1906.01916, Jun 2019.
- [15] Antti Tarvainen and Harri Valpola, "Mean teachers are better role models: Weight-averaged consistency targets improve semi-supervised deep learning results," in *Advances in neural information processing systems*, 2017, pp. 1195–1204.
- [16] Geoffrey French, Michal Mackiewicz, and Mark Fisher, "Self-ensembling for visual domain adaptation," *arXiv preprint arXiv:1706.05208*, 2017.
- [17] Qiao Hu, Michael D Abramoff, and Mona K Garvin, "Automated separation of binary overlapping trees in low-contrast color retinal images," in *International conference on medical image computing and computer-assisted intervention*. Springer, 2013, pp. 436–443.
- [18] Jan Odstreilik, Radim Kolar, Attila Budai, Joachim Hornegger, Jiri Jan, Jiri Gazarek, Tomas Kubena, Pavel Cernosek, Ondrej Svoboda, and Elli Angelopoulou, "Retinal vessel segmentation by improved matched filtering: evaluation on a new high-resolution fundus image database," *IET Image Processing*, vol. 7, no. 4, pp. 373–383, 2013.
- [19] José Ignacio Orlando, Joao Barbosa Breda, Karel Van Keer, Matthew B Blaschko, Pablo J Blanco, and Carlos A Bulant, "Towards a glaucoma risk index based on simulated hemodynamics from fundus images," in *International Conference on Medical Image Computing and Computer-Assisted Intervention*. Springer, 2018, pp. 65–73.
- [20] Meindert Niemeijer, Xiayu Xu, Alina V Dumitrescu, Priya Gupta, Bram Van Ginneken, James C Folk, and Michael D Abramoff, "Automated measurement of the arteriolar-to-venular width ratio in digital color fundus photographs," *IEEE Transactions on medical imaging*, vol. 30, no. 11, pp. 1941–1950, 2011.